Date of publication xxxx 00, 0000, date of current version xxxx 00, 0000.

Digital Object Identifier 10.1109/ACCESS.2021.DOI

Experimental evaluation of RF waveform designs for Wireless Power Transfer using Software Defined Radio

SUMIT GAUTAM[†,1,2], (Member, IEEE), SUMIT KUMAR[†,1], (Member, IEEE), SYMEON CHATZINOTAS[1], (Senior Member, IEEE), and BJÖRN OTTERSTEN[1], (Fellow, IEEE)

[1]Interdisciplinary Centre for Security, Reliability and Trust (SnT), University of Luxembourg, L-1855 Luxembourg.
[2]Huawei Technologies Sweden AB, Vädursgatan 5, 412 50 Göteborg, Sweden.
[†] These authors have contributed equally to this work.

Corresponding author: Sumit Kumar (e-mail: sumit.kumar@uni.lu).

The research leading to these results has received funding from the Luxembourg National Research Fund (FNR), Luxembourg, under the FNR-FNRS bilateral - InWIP-NET: Integrated Wireless Information and Power Networks (R-AGR-0700-10-X).

ABSTRACT The possibility to harvest energy from ambient radio-frequency (RF) sources has intrigued humankind for the past several decades. In this context, there has been a tremendously growing research interest in the field of wireless power transfer (WPT) using the RF range of the electromagnetic (EM) spectrum. In this paper, we experimentally investigate the aspect of real-time energy harvesting (EH) via different types of waveform designs such as orthogonal frequency division multiplexing (OFDM), square, triangular, sinusoidal, and sawtooth. We make use of a Software Defined Radio (SDR) and a Powercast P21XXCSR-EVB EH module to carry out the experiments on a practical device to assess performance. Specifically, we are interested in obtaining some insights based on the comparison between the aforementioned waveform designs from the perspectives of the separation distance between the USRP and P21XXCSR-EVB EH module, and power emission via USRP. In this vein, we perform additional subsequent experiments after reporting the practical effectiveness of the OFDM waveform, which also follows our intuitive analysis. Correspondingly, we study the effect on WPT with variable USRP transmit power, the separation distance between the USRP and EH antennas, number of OFDM sub-carriers, and multipath setting. As an application of OFDM, the effectiveness of fifth generation-new radio (5G-NR) and long-term evolution (LTE) waveforms are also tested for the WPT mechanism. The demonstration of the EH is provided in terms of the above-mentioned investigation metrics while seeking the best waveform to support WPT.

INDEX TERMS Fifth Generation-New Radio (5G-NR), Long Term Evolution (LTE), RF-Energy Harvesting, Universal Software Radio Peripheral (USRP) - Software Defined Radio (SDR), Wireless Power Transfer (WPT).

I. INTRODUCTION

WITH each passing year, we are inching closer and closer towards realizing a smart and connected society. In the process, it is important to note the increasing presence of low-power consuming internet-of-things (IoT) devices. These devices primarily serve the purpose of data collection in the form of various types of sensors (e.g., temperature, pressure, etc.), however, bounded by the strict battery limitations. To address the battery charging issues where the devices are placed at very remote places, while also taking into consideration the data exchange process; the possibility to use radio-frequency (RF) signals as a wireless charging means along with the traditional information transmission has gained due attention [1].

Recent research and developments in the area of wireless power transfer (WPT) using RF signals have focused on laying important theoretical foundations pertaining to several key aspects in the domain, such as waveform designing, rectifier-based modeling, beamforming algorithms, coexistence with traditional wireless communications systems, etc., [2]. While the theoretical findings motivate the use of multi-sine type waveform designs (e.g., Orthogonal Fre-

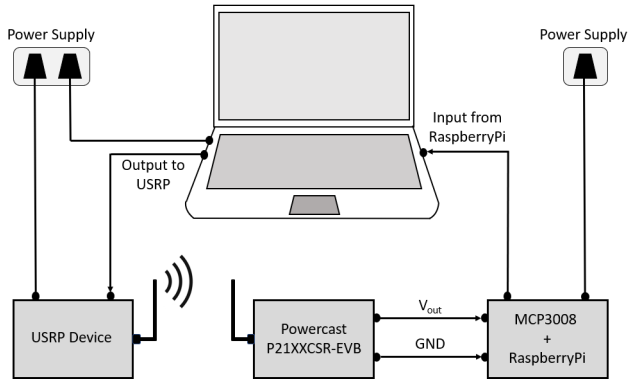

FIGURE 1. System set-up for wireless experiments comprised of a laptop, USRP, Powercast P21XXCSR-EVB energy harvester, MCP3008 and RaspberryPi.

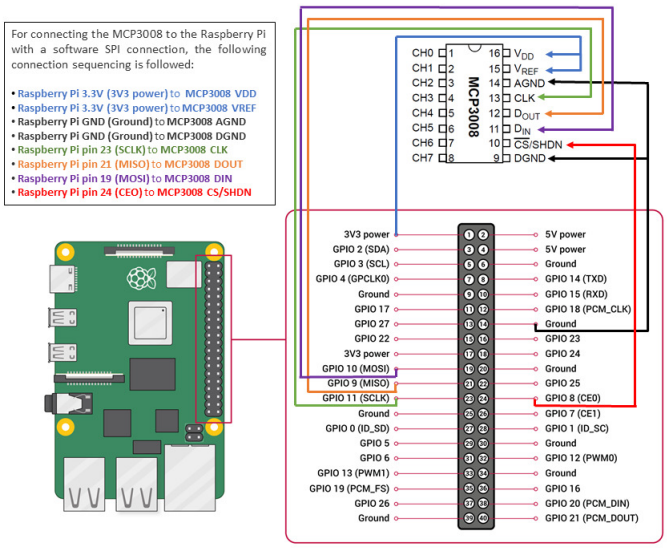

FIGURE 2. Connection diagram between MCP3008 and RaspberryPi for interpreting V_{out} from the Powercast P21XXCSR-EVB.

quency Division Multiplexing (OFDM)) for WPT [2], recent experimental findings still back the adoption of traditional Sinusoidal waveform in the 915 MHz operation regime [3]. Additionally, the square waveform [4] and extended square, i.e., rectangular waveform [5] are also potential candidates to be considered as possible inputs for efficient WPT.[1] The authors in [6] investigated single sinusoid RF waveforms which yielded the highest DC-DC and receiver efficiency, whereas several unconventional waveform designs were investigated in [7]. In this context, seeking the best suitable waveform design for WPT is important, which is the main focus of this work.

Over the years, there have been several interesting contributions in the area of communications and system design [8]–[10] targeting optimization of the end-to-end transmission in RF WPT, some of which are well summarized in [2]. Considering the co-phased multi-sine waveform, the researchers in [2], [7]–[9] provided an interesting insight on the suitability of the waveform transmission at a high peak-to-peak average power ratio (PAPR) over a flat fading channel. In this context, the challenges arising due to high PAPR signal generations can be addressed using spatial combining techniques [11], [12]. The developments in [2], [7], [8] motivate the use of high-PAPR signals for an efficient WPT process over a flat fading channel. It is noteworthy that most of the relevant works in the literature are only backed by a theoretical rigor, with no clear distinction/agreement on the use of any particular waveform for WPT without practically tested a variety of waveforms. In addition, the idea of using different waveforms for information and energy transmissions seems interesting, but its practical tractability is questionable. Therefore, it seems to be in the best of interest for the researchers to seek suitable waveforms among the existing ones (in practice) to support WPT, especially from the perspective of practical hardware deployments by network operators. However, a unanimous outcome from these works suggests the adoption of an impulsive train type of waveform to facilitate WPT with maximum efficiency.

In this paper, we present a comparison between five different types of traditional waveform designs by performing Over-The-Air(OTA) real-time Radio Frequency transmissions to bring more clarity on the best type of waveform design that is suitable for the WPT mechanism. We perform an experimental analysis of the output voltage measurement obtained from the Powercast P21XXCSR-EVB energy harvesting (EH) module, where the WPT process is facilitated by a Software Defined Radio (SDR) transmitter. We use SDR because using the same hardware, and just by changing the software, a multitude of waveforms can be generated and transmitted with full gain over transmission frequency and power. The SDR transmits the considered waveform designs over a wireless medium (and later via an equivalent wired medium with attenuator), which are individually utilized to test the efficacy of the WPT mechanism. Concerning the EH module, it is noteworthy that the amount of harvested energy may be estimated either via the charging of an energy-storage battery element or a capacitor. The presence of the latter component in the EH module enables us to investigate its charging and discharging cycles through the time series of voltage values.[2] Herein, a constant voltage supply (as a result of the extremely high frequency of peaks) would be more desirable for the charging operation. Ideally, we aim to identify a suitable waveform candidate which can provide frequent peak values of the voltage for the capacitor to charge swiftly and continue to stay in the charged state for the whole duration of the transmission.

Further sections of this paper are organized as follows. Section II provides an introduction to the system model comprising the hardware and software specifications. The

[1]Noticeably, the energy captured via any type of waveform is largely dependent on the arrangement of passive RF components in the EH module.

[2]Note that the voltage is directly proportional to the received power.

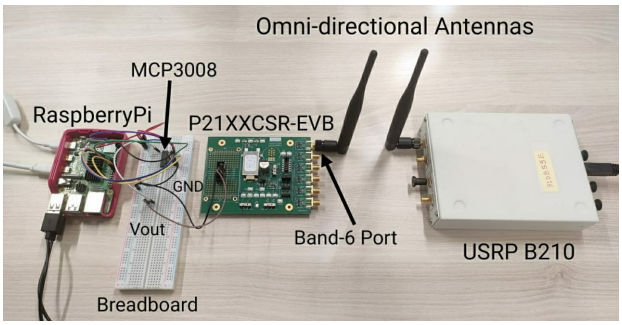

FIGURE 3. Experimental set-up for analyzing WPT via various waveform designs transmitted over wireless medium using an SDR. Note that the depicted figure is meant for illustration purposes and the separation distance between the transmit and receive antennas might vary during the experimentation phase depending on the USRP transmit power.

details on real-time on-board evaluation and corresponding analysis are presented in Section VI. Discussions on major outcomes are presented in IV, followed by concluding remarks in Section VIII.

II. SYSTEM SET-UP – I : HARDWARE AND SOFTWARE

In this section, we describe the system model for the first part of our experimentation in detail. Our experimental set-up is comprised of a general-purpose CPU(laptop), Universal Software Radio Peripheral (USRP) B210 SDR, 2.45 GHz omnidirectional antennas, Powercast P21XXCSR-EVB EH module, MCP3008 ADC, and a RaspberryPi. The laptop provides instructions to the USRP pertaining to the chosen waveform and corresponding wireless emission. The USRP then emits the waveform over the wireless medium for the EH module to harness its energy from. Since the output readings from the EH module are in an analog form, we make use of MCP3008, which is a 10-bit Analog-to-Digital Converter (ADC). The ADC is interfaced to the RaspberryPi, which logs the digital data results for further interpretation. The schematics for the overall system model and interconnection between the MCP3008 and RaspberryPi are shown in Fig. 1 and Fig. 2, respectively. A snapshot of the experimental set-up is provided in Fig. 3. Further descriptions of the involved equipment are discussed below.

TABLE 1. Equipment details related to the system set-up.

Equipment	Details
Laptop	Dell Latitude 5490, 16GB RAM, Core i7, Ubuntu 18.04, GNU Radio Version 3.7
SDR	USRP B210: Ettus Research-National Instruments.
Antennas	2.45GHz, Omnidirectional, Gain: 3dBi
RF-EH Module	Powercast P21XXCSR-EVB
MCP3008	10-bit Analog-to-Digital Converter(ADC),150 Ksps
RaspberryPi	Version 4, Python Ver-3 data from ADC
Connectors	Laptop to USRP: USB3.0, EH module to ADC & ADC to RaspberryPi: normal jumper cables, RaspberryPi to Laptop: Ethernet Cat5.

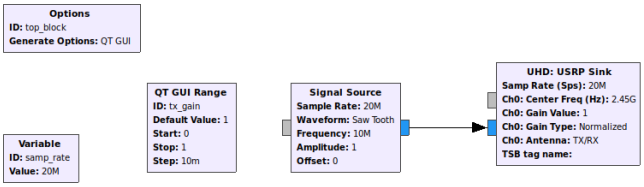

FIGURE 4. GNU Radio GUI programming environment

A. USRP AND GNU RADIO

For our experiments, we make use of the Ettus USRP B210 SDR [13] hardware. It is a dual-channel Field Programmable Gate Array (FPGA) based transceiver with a frequency span of 70 MHz - 6 GHz and provides 56 MHz of real-time bandwidth. Using an SDR enables us to transmit a variety of waveforms using the same hardware. To transmit different waveforms, we use dual-band omnidirectional antennas Vert-2450 [14] which have a frequency range of 2.4-2.5 GHz and 4.9-5.9 GHz. On the software side, we used GNU Radio [15] which is used to program the USRP B210 SDR and design multiple waveforms. Under GNU Radio, waveforms are designed using a Graphical User Interface (GUI) based environment as shown in Fig. 4. We have used five different waveform designs: (i) square, (ii) triangle, (iii) sinusoidal, (iv) saw-tooth, at a sampling rate of 20 MHz and baseband frequency of 10 MHz, and (v) OFDM at a sampling rate of 20 MHz and 64 point FFT. For OFDM, we used the gr-ieee802-11 package of GNU Radio which is capable of generating standard-compliant IEEE 802.11g waveforms [16]. Analog gain of the waveforms is controlled on the fly using GNU Radio GUI during transmission.

B. POWERCAST P21XXCSR-EVB EH MODULE

The multi-band enabled Powercast P21XXCSR-EVB EH module provides six frequency band options to harvest energy from: GSM-850 uplink, Europe RFID & GSM-850 downlink, ISM USA & GSM-900 uplink, GSM-1800, GSM-1900 uplink, and Wi-Fi 2.4GHz. We use the Band 6 (Wi-Fi 2.4GHz) and choose Capacitor C6, with DEFAULT switch mode in S1. The switch S2 is kept in the OFF position while S3 is kept at MEAS/VCC. The default maximum output voltage i.e., V_{out} for this setting is 3.3 Volts [17], [18].

TABLE 2. Software/Parameter stipulations for experiments.

Feature	Specifications
Frequency Band	802.11g - 2.4 GHz
Carrier Frequency	2.45 GHz
Sampling Rate	20 MHz
Baseband Frequency	10 MHz
OFDM Details	64 (52 sub-carriers utilized, 11 Guard-band & 1 DC, BPSK)
Sample tapping rate	100 samples collected per second
RF-EH Settings	Band 6, Capacitor : C1, S1 : DEFAULT, S2 : OFF, S3 : MEAS/VCC

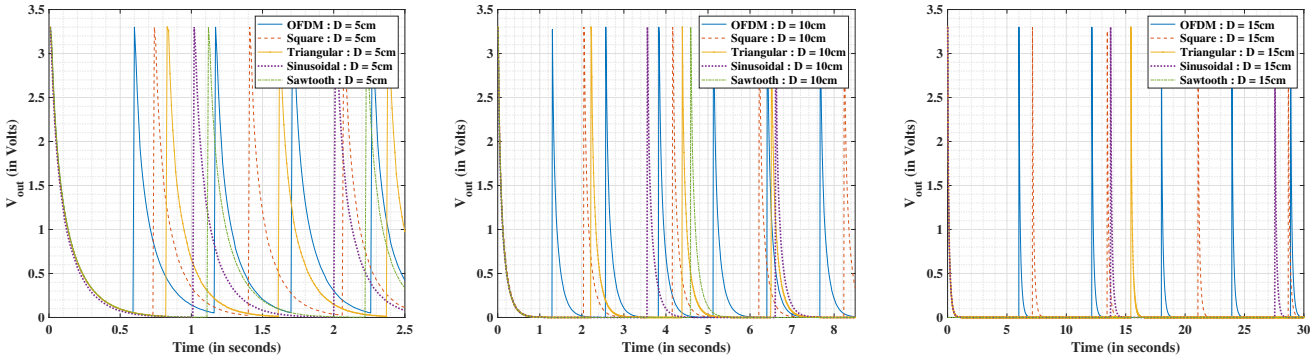

FIGURE 5. Comparison between the peak-to-peak V_{out} obtained via considered waveform designs: OFDM, square, triangular, sinusoidal, and sawtooth, for a separation distance between the USRP and P21XXCSR-EVB EH module (a) D = 5cm, (b) D = 10cm, and (c) D = 15cm. We observe that as the distance increases, the charging time also increases, besides, OFDM outperforms all other waveforms in terms of charging time.

C. MCP3008 ADC

To interpret the results from the EH module, i.e., V_{out}, we need MCP3008 [19] to convert the received analog output into digital form. The 10-bit ADC provides a maximum value of 1023 in our experiment, which corresponds to 3.3 Volts. The V_{out} from the EH module may be connected to any of the channels (CH0-CH7) of MCP3008. For our experiment, we use the CH0 to interpret the results via RaspberryPi.

D. LOGGING DATA VIA RASPBERRYPI

We use the RaspberryPi v4 [20] to log the voltage values produced by the considered EH device. MCP3008 is interfaced to the RaspberryPi and digitized voltage values from CH0 are obtained through the Serial Programming Interface (SPI). We use Python to write the data-logging script and set the sampling rate of MCP3008. For our experiments, we assume a sampling rate of 100 samples per second (SPS), which is sufficient for our purpose.

More details on the equipment and parameter selections for software configuration are provided in Table I and Table II, respectively. In the succeeding section, we discuss the considered experimental findings and corresponding analysis.

III. REAL-TIME ON-BOARD EVALUATION AND ANALYSIS - PART I

For the hardware experiments, we use the Industrial Scientific and Medical (ISM) band of 2.4 GHz, where the center frequency of 2.45 GHz is considered. The transmitted waveforms are generated at a sampling rate of 20 MHz and the corresponding IQ samples are sent to the USRP through a USB3.0 cable. The USRP transmits the waveform over the wireless medium. The USRP and the EH antennas are separated by a short distance. This is because the USRPs are designed for institutional use are limited by extremely small maximum transmit power. Besides, we did not use a power amplifier for our experiments otherwise the ambient WiFi network would have been affected (as we are using 2.45GHz). We use GNU Radio normalized gain knob which maps the span of the entire gain of USRP between 0 to 1. The measured values for each waveform corresponding to 100% of the peak transmitted power(,i.e., normalized gain of 1) by the USRP are measured as follows: OFDM (-23 dBm), square (-19 dBm), triangular (-18 dBm), sinusoidal (-14.75 dBm), and sawtooth (-18.4 dBm). [3]

The experiments are performed in real-time OTA on the specified system setup. We evaluate the effects of increasing the distance and transmit power on the received V_{out} from the EH module. Specifically, the interpretation of results is primarily dependent on the charging and discharging cycles of the capacitor present in the EH module. In this context, it is noteworthy that the peak-to-peak voltage values will differ according to the type of waveform chosen at the transmit node, i.e., USRP. From a real-time perspective, it is difficult to start the experiment from one peak itself. Hence, we start the collection of samples at any random time after the USRP starts the transmission process. In the process, we collect 100 samples per second with a maximum of 5000 sample collections. After logging the outcomes, we align the first peaks corresponding to the various waveform designs for the experiments. This alignment facilitates in better interpretation of the results. In the following, we present the results and discussions related to the WPT based on the variation of distance between the USRP and EH module, and the transmit power metric at the USRP.

A. IMPACT ON WPT BY VARYING THE SEPARATION DISTANCE BETWEEN THE USRP AND POWERCAST P21XXCSR-EVB EH MODULE

From an intuitive viewpoint, it is easy to interpret the effect of increasing the separation distance between the transmitter and EH module, on WPT. Concretely, the analysis of RF-enabled wireless communications systems provides a better understanding of the fate of wireless signals with specific

[3] An intuition-based discussion on the effect of the considered waveforms is provided in Appendix A.

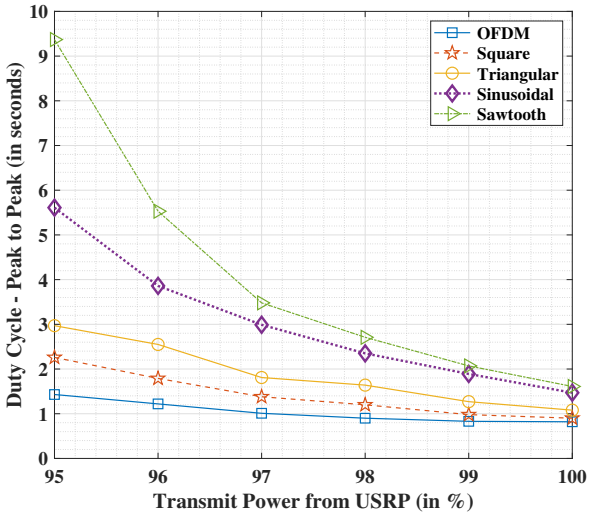

FIGURE 6. Effect of varying transmit power from the USRP on the Duty Cycle - Peak-to-Peak for the considered waveform designs. We observe that the Duty-Cycle for OFDM is least compared to other waveforms which indicate the lesser charging time.

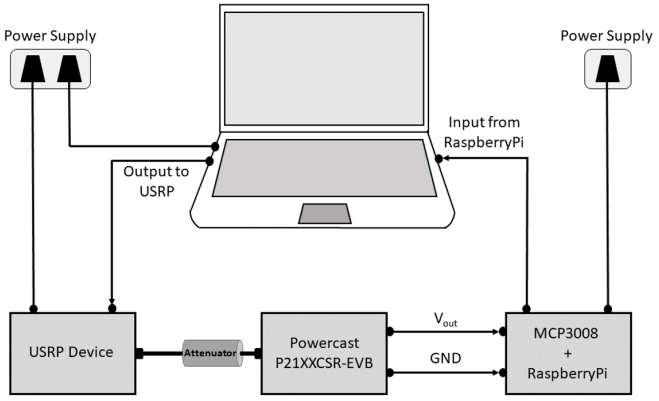

FIGURE 7. Updated system set-up comprising previously defined equipment, while introducing additionally wired(SMA cable) connection with attenuator between the USRP and EH module.

waveform and power. Due to the environmental penetration losses, the overall received wireless signal becomes weak and gets weaker with the increasing separation distance between the transmitter and receiver. This is well explained by the Friis transmission formula for the free space path loss [21]

$$\frac{P_T}{P_R} \propto \frac{1}{D^2}, \tag{1}$$

where P_T is the transmit power, P_R is the received power at the receiver and D is the separation distance between the transmit antenna and receive antenna. In our experiment, P_T is the transmit power from the USRP (kept at 100%), P_R is the received power at the EH module and D is the separation distance between the antennas of the USRP and EH module.

In Fig. 5, we show the effect of increasing the distance on the harvested energy via various considered waveforms, viz-a-viz., OFDM, square, triangular, sinusoidal, and sawtooth. We observe that the separations between the peak-to-peak voltages obtained at the receiver via each corresponding waveform continue to grow with increasing separation distances between the antennas of the USRP and EH module.[4] Further, it is noted that the peaks appear less frequently with increasing separation distance, indicating that the capacitor requires higher time to charge at its peak. In terms of the waveform designs, we observe that OFDM is the best suitable multi-carrier candidate among all the chosen waveform designs for comparison, while the square waveform is found to be the best suitable single carrier waveform candidate for facilitating the EH process in all the cases.

[4]Note that short separation distances are considered for investigation since power amplifiers are not used during the transmission process from USRP.

B. IMPACT ON WPT WITH VARYING THE TRANSMIT POWER OF USRP

It is a well-known fact that an increase or decrease in the transmit power causes the same corresponding effect at the receiving node. This implies that the received power increases with growing transmit power values and vice-versa, while the path-loss phenomenon mentioned in (1) also holds. In this context, we perform our experiments by keeping a fixed separation distance between the antennas of the USRP and EH module with D = 7.5cm, while changing the transmit power values at the USRP device. In the process, we take into consideration the sample differences (SD) between the first peak and second peak of V_{out} for each of the considered waveform designs. This indicates the charging-discharging cycles of the capacitor present in the EH module, which we term as the Duty Cycle - Peak-to-Peak calculated as SD per 100 received SPS.

We report in Fig. 6 the effect of varying transmit power from the USRP on the Duty Cycle - Peak-to-Peak for the considered waveform designs. In line with the above-mentioned intuitive discussion, we find that the Duty Cycle for the capacitor decreases with the increase in the transmit power from the USRP. This also indicates a faster charging process and the waveform with the least Duty Cycle at any value of transmit power would be considered most suitable for the EH mechanism. We note that in this case, OFDM outperforms the other considered waveform designs from the multi-carrier perspective, while the square wave is found to be the most suitable candidate for the EH process from a single carrier viewpoint.

C. FURTHER EXPERIMENTATION WITH OFDM

From the results reported in the previous section, it is clear that the OFDM waveform is found to be the best amongst all the considered waveforms to facilitate WPT. However, we note the possibility of having a deteriorated signal received at the EH module undergoing a multi-path effect considering a

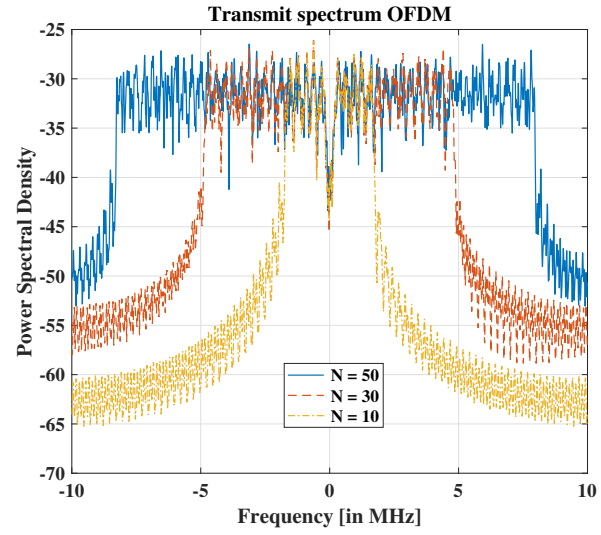

(a)

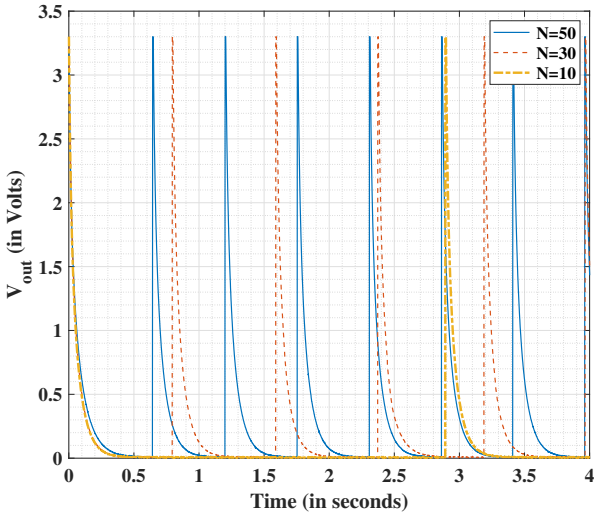

(b)

FIGURE 8. (a) Spectrum of OFDM waveform with varying number of occupied sub-carriers (50, 30 and 10), and (b) Effect on EH with varying number of OFDM sub-carriers. We observe that as the number of occupied sub-carriers in an OFDM waveform is reduced, the charging time also increases.

practical scenario. Therefore, we alter our experimental set-up slightly by introducing a wired connection between the USRP (emitting 90% of the peak transmit power) and the EH module, to not only address the above-mentioned challenge but also to provide another perspective in carrying out the further experiments. It is noteworthy that the corresponding path-loss factors can be introduced using different values of an attenuator (α), which thereby helps in emulating a static multipath wireless channel. More specifically, an equivalent wireless channel may be emulated using the set-up described herein and as shown in Fig. 7, for cases wherein the wireless transmission is not possible for carrying out the experiment. Following the above discussion, we investigate the performance of OFDM facilitating WPT from two perspectives, namely, variation in the number of OFDM sub-carriers, and variation in the attenuator values(,i.e., path loss values of different multipath). The corresponding results are discussed in the subsequent sections.

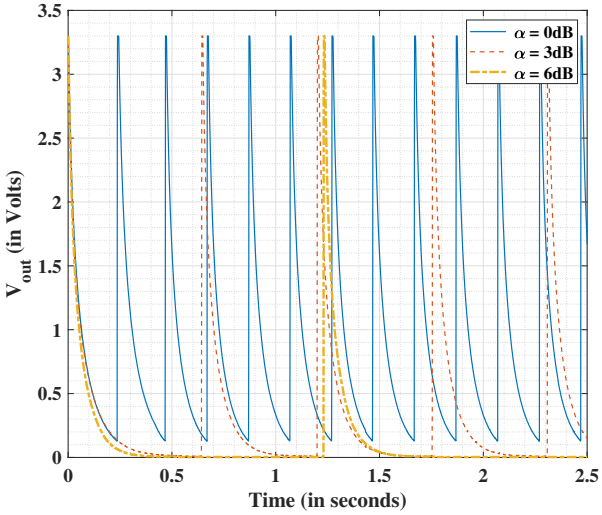

FIGURE 9. Comparison between the peak-to-peak V_{out} obtained via different attenuator values with N = 50 (fixed sub-carriers in-use). We observe that for a fixed transmit power as the signal is attenuated, the charging time of the EH circuit also increases. Here the attenuation represents the path loss.

1) Effect on WPT with varying number of OFDM sub-carriers

Based on the inherent properties of OFDM, one well-established property is that a large number of sub-carriers in-use (N) provides significant system gains [22]. More specifically, multiple sub-carriers help in better management of resources at the desired user in comparison to a single carrier case. Intuitively, a similar notion must hold in the case of WPT. In this regard, we make use of the set-up mentioned in the previous section while considering a wired connection with an attenuator (α = 3dB) to emulate a wireless scenario having D = 1.5 cm (approximately, assuming the transmit and receive gains of 0dB each).[5] In Fig. 8, we show the effect of varying the values of N on the WPT. Herein, we observe that a large number of OFDM sub-carriers are beneficial for the WPT operation as well. For our experiments, we used a maximum of 64 sub-carriers, however, the benefits of utilizing a large number of OFDM sub-carriers for WPT are explicit. In the following section, we provide the experimental analysis for WPT by introducing variable attenuators (to emulate D as in the wireless setting).

[5]The value of D corresponding to α may be obtained by using the free-space path loss expression [21].

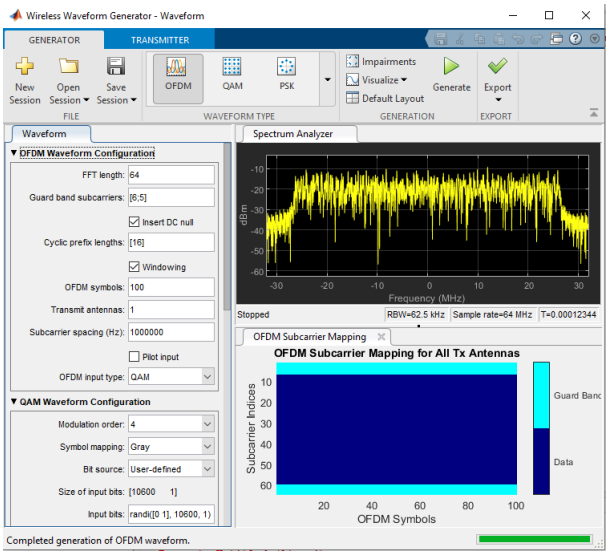

FIGURE 10. Wireless Waveform Generator Toolbox from MATLAB 2021a which is used for the waveform generation in our experiments.

2) Analysis with the incorporation of variable attenuators

In this section, we consider the aspect of introducing various values of α to test the efficacy of the OFDM signal with N = 50. As investigated before, significant signal power loss is observed with the increasing separation distance between the USRP device and the EH module. Herein, it is noteworthy that the introduction of various values of α essentially translates to different corresponding possibilities of D. To carry out this part of the experiment, we assume the same set-up as above, however, with the assumption of N = 50 to be tested for different values of α. The results illustrated in Fig. 9 show the effect of varying values of α on the WPT process. Clearly, the received signal power reduces significantly with increasing values of α (or D in the case of wireless scenario). Since most practical systems employ the OFDM-based standards to facilitate data, therefore the proposed framework seems promising from the practical application viewpoint. Moreover, it will be interesting to carry out further analysis in regards to the consideration of adequate center frequency for facilitating the WPT process. The corresponding investigation is carried out in the subsequent sections.

IV. MAJOR OUTCOMES, APPLICATIONS AND INTERPRETIVE DISCUSSION - PART I

Based on our experiments, we find that the OFDM waveform (similar to multi-sine) is found to be the best suitable candidate among all the considered waveform designs, viz., OFDM, square, triangular, sinusoidal, and sawtooth. However, the square waveform also provides an appreciable performance in the single carrier waveform category. The efficiency of the multi-carrier OFDM waveform is justified by the fact that the EH module sees the multi-sine waves as the supplier of frequent peak voltages, which improves the charging process at the capacitor placed in the EH module. Surprisingly, the triangular wave is found to provide better performances in comparison to the sinusoidal wave for several investigative instances. In contrast, the sawtooth wave performs the worst due to obvious reasons of not being able to provide frequent peak-to-peak voltage values. Since multi-carrier systems with a high number of sub-carriers may resemble a continuous high-frequency square wave, therefore it is needless to mention that such waveform designs which provide highly frequent peak-to-peak voltage values are to be considered the best for the EH mechanism. As an interesting trade-off, this phenomenon appears to be the opposite of what we want for a normal information transmitter to avoid non-linear distortion. Towards this end, we established that the usage of a higher number of ODFM sub-carriers is found to be beneficial for the WPT process. In addition, we showed the distance limitations (based on variable α values) of OFDM for WPT operation at the central frequency of 2.45 GHz.

From a practical implementation perspective, the proposed experiments seem promising primarily because of the establishment of the OFDM signal as a suitable candidate waveform for facilitating WPT. Unlike the common notion of having different waveforms for information and power transfer respectively, the outcomes of this work motivate towards the consideration of already existing transmission methodologies incorporating OFDM for simultaneous wireless information and power transmission (SWIPT). In this vein, several scenarios pertaining to OFDM properties (incorporating a high number of sub-carriers and various modulation schemes) such as finding a suitable central frequency for facilitating WPT, and examining the effects of multi-path (via emulated wireless scenario) on WPT remain open areas for investigation. Moreover, the WPT characteristics are required to be tested for the OFDM-based waveforms adopted in the fifth-generation new radio (5G-NR) and fourth-generation Long Term Evolution (LTE) [23], [24]. Additionally, we further intend to test the efficacy of variable numerologies based on the 5G-NR waveform and the traditional LTE waveform having OFDM with a fixed sub-carrier spacing of 15 kHz, given that the OFDM is found to be the best waveform to assist the WPT process.

V. SYSTEM SET-UP – II : HARDWARE AND SOFTWARE

In this section, we describe the considered system model for the second part of our experimentation in detail. For the experimental verification and RF testing, we again used two different USRP SDRs with different capabilities. USRP B210

TABLE 3. Equipment details related to the system set-up.

Equipment	Details
Desktop	i9-10900K CPU (3.70GHz), 64GB RAM, Ubuntu 18.04, GNU Radio Version 3.7
SDR	USRP B210, N310
RF-EH Module	Powercast P21XXCSR-EVB
MCP3008	10-bit Analog-to-Digital Converter(ADC),150 Ksps
RaspberryPi	Version 4, Python Ver-3 data from ADC

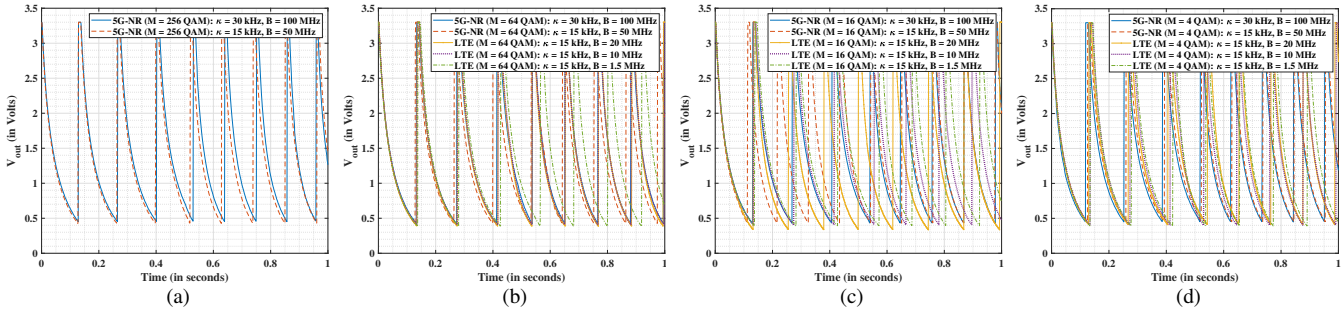

FIGURE 11. Considering the maximum USRP transmit power τ = 80%, we show the comparisons between the various types of 5G-NR and LTE waveforms, following the modulation schemes: (a) 256 QAM, (b) 64 QAM, (c) 16 QAM, and (d) 4 QAM.

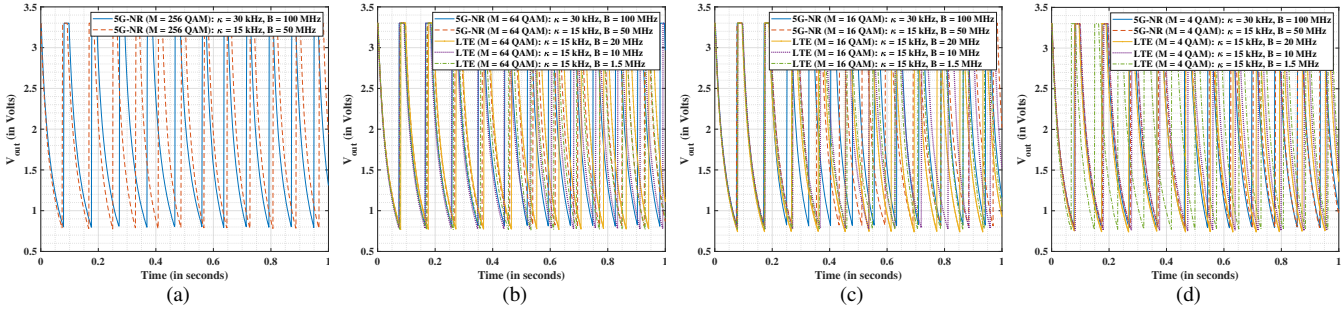

FIGURE 12. Considering the maximum USRP transmit power τ = 90%, we show the comparisons between the various types of 5G-NR and LTE waveforms, following the modulation schemes: (a) 256 QAM, (b) 64 QAM, (c) 16 QAM, and (d) 4 QAM.

(70 MHz - 6 GHz, SR: 61.44 Msps) is used for Non-5G waveforms while USRP N310 (10MHz - 6GHz, SR: 61.44, 122.88 Msps) is used for 5G-NR waveforms as the former USRP does not support the sampling rate of 122.88 Msps which is required for the 30 kHz SCS in 5G-NR waveform. Powercast P21XXCSR-EVB is used as an EH module from which the output voltage and harvested energy are captured using MCP3008 ADC and RaspberryPi. Unless specified otherwise, we choose τ = 70% and α = 3dB to carry out the further experiments. The connection diagram is the same as shown in Fig. 7. The other relevant details are described in Table 3 and Table 4.

VI. REAL-TIME ON-BOARD EVALUATION AND ANALYSIS - PART II

Following the updated system model described in the previous section, we present herein some additional experiments

TABLE 4. Software/Parameter stipulations for experiments.

Feature	Specifications
Carrier Frequency	2.45 GHz, 915 MHz
Sampling Rate	20 MHz
Baseband Frequency	10 MHz
OFDM Details	64 (52 sub-carriers utilized, 11 Guard-band & 1 DC, BPSK)
Sample tapping rate	1000 samples collected per second
RF-EH Settings	Band 3, Band 6, Capacitor : C1, S1 :DEFAULT, S2 : OFF, S3 : MEAS/VCC

based on OFDM, specifically concerning the 5G-NR and 4G LTE waveforms, the comparison of the different center frequency of operations, and an investigation based on the multipath effects. In the following, we first proceed with performing experiments with the 5G-NR and 4G LTE waveforms to investigate the WPT efficacy of the corresponding waveforms.

A. APPLICATIONS OF OFDM: EXPERIMENTATION WITH 5G-NR AND LTE WAVEFORMS

From the discussions presented in the previous sections, we note the effectiveness of the OFDM waveform in facilitating the WPT process. Noticeably 5G-NR waveforms are also based on OFDM, however, in contrast to 4G LTE (which also uses OFDM for its downlink), the subcarrier-spacing (SCS) is flexible in 5G-NR OFDM waveforms. Therefore, it is interesting to carry out an investigation to test the effectiveness of 5G-NR and LTE waveforms. To proceed, we discuss the process for generating the 5G-NR and LTE signals and provide a corresponding analysis followed by an interpretative discussion in the subsequent sections.

1) Process of generating the waveforms

For the generation of waveforms, we used the Wireless Waveform Generator Toolbox from MATLAB. The toolbox enables the generation of OFDM waveforms with different subcarrier spacing, sample rates, data sequences, etc. Once a particular waveform (complex sequence) is generated, it

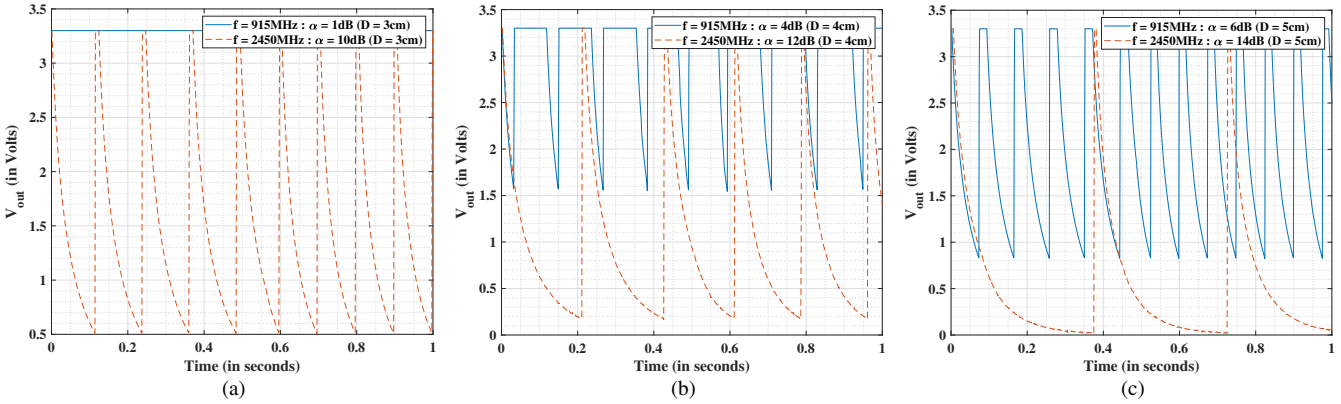

FIGURE 13. Comparison of OFDM transmissions for variable emulated distances: (a) $D = 3$cm, (b) $D = 4$cm, and (c) $D = 5$cm, with the central frequencies: (i) $f = 915$ MHz and (ii) $f = 2.45$ GHz, to investigate the WPT process. We observe that at lower frequency, the charging of EH is more frequent in comparison to the relatively higher frequency.

is exported as a binary file where we save the In-phase (I) and Quadrature (Q) components with 16 bit each. Further, we use GNU Radio scripts to read the binary waveform and push them into USRP for their transmission in the wireless medium. An illustration of the MATLAB Waveform Generator Toolbox with relevant options are shown in Fig. 10. In the following, we provide and discuss some more details on further experimentation.

2) Experimental Results

After having discussed the process of generating 5G-NR and 4G LTE waveforms, we present some experimental results in this section based on variable USRP transmit power (τ) and different modulation schemes, denoted by M. Let κ represent the sub-carrier spacing between the OFDM sub-carriers, and B denote the bandwidth. Considering Fig. 11 and Fig. 12, the (a) part of the experiments consider 5G-NR waveforms only with M = 256 QAM and two standard numerologies namely, κ = 30 kHz, B = 100 MHz, and κ = 15 kHz, B = 50 MHz. In the (b) part of Fig. 11 and Fig. 12, we consider M = 256 QAM with two 5G-NR numerologies (mentioned as above) and three possibilities of 4G LTE-based transmissions (κ = 15 kHz) viz., (i) B = 20 MHz, (ii) B = 10 MHz and (iii) B = 1.5 MHz. With the considerations of the five above-mentioned types of waveform possibilities, we perform experiments by choosing M = 16 QAM and M = 4 QAM in the (c) and (d) parts of both Fig. 11 and Fig. 12, respectively. The difference between the results of Fig. 11 and Fig. 12 are primarily based on the variation in τ values. We note that the EH process becomes better with increasing τ values, following the results which show more frequent peaks of waveforms in Fig. 12 compared to Fig. 11. However, we note that all the considered waveforms perform nearly equal in terms of the WPT process keeping in mind the practical hardware imperfections, where no significant difference is observed in the performance. We provide an interpretative discussion on some other possibilities in the following section.

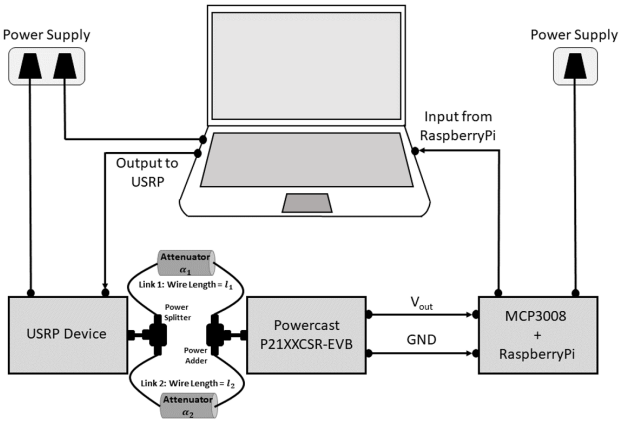

FIGURE 14. System set-up to emulate wireless multipath scenario. Different length of the SMA cable provides phase difference between the two paths, while the path gain is achieved through attenuators.

3) Interpretative Discussion

As noted from the results obtained in Fig. 11 and Fig. 12, we find that there is a subtle variation in the EH via chosen 5G-NR and 4G LTE waveforms. However, this separation may become wider when considering external factors like extended time periods, signal power loss in the environment, the separation distance between the transmitter and end-user, and consideration of different central frequencies. Therefore it is difficult to comment on the best waveform among the chosen 5G-NR and 4G LTE options, which altogether provides highly efficient EH. Further analysis is however an open area of research and can be considered in future works. In the following section, we discuss another perspective for carrying out our experiments with consideration of different carrier center frequencies to assist the WPT process.

B. COMPARISON OF OFDM TRANSMISSION AT DIFFERENT CENTRAL FREQUENCIES

In this section, we compare the effect of changing the center carrier frequency of OFDM on the WPT process. To proceed, we make use of the band-3 and band-6 of the EH module.

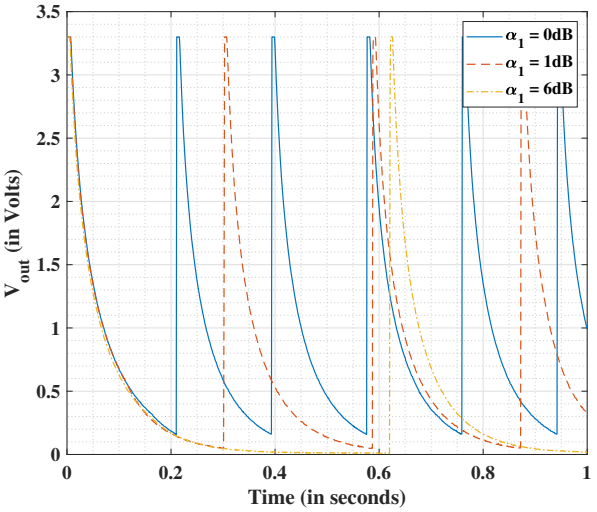

FIGURE 15. The effect of multipath in wireless scenario is emulated with the help of various considerations of α_1, and α_2 = 0dB. With α_1, and α_2 representing the gain difference between the two paths, we observe that as the gain difference between the two paths increases, the charging time increases.

We set τ = 70% and vary the values of α to carry out our experiments with OFDM waveform emitted towards the EH module at central frequencies f = 915 MHz and f = 2.45 GHz. The corresponding values of α with respect to considered separation distances of (a) D = 3cm, (b) D = 4cm, and (c) D = 5cm, are chosen according to the free-space path loss expression [21].[6] The respective results reported in Fig. 13 (a), Fig. 13 (b) and Fig. 13 (c) show the WPT performance benefits on the use of f = 915 MHz central carrier frequency over f = 2.45 GHz for all variations of α. It is explicit that the charging of the capacitor is more frequent for a waveform with f = 915 MHz center carrier frequency over f = 2.45 GHz because of low path-loss in the former in comparison to the latter. As expected, the WPT efficiency reduces considerably when the separation distance between the transmitter and end-user is increased (virtually with the help of an adequate selection of α). However, it is noteworthy that the effect of multipath may become prominent (in the completely wireless scenario) at large values of D. Therefore, this calls for an additional set of experiments to study the effect of multipath on the WPT efficiency, which is presented in the next section.

C. INVESTIGATION OF MULTIPATH EFFECT ON WPT

In this section, we perform experiments to emulate a multipath scenario experienced by OFDM signals in an equivalent wireless multipath medium and investigate the corresponding effect on the WPT process. As shown in Fig. 14, we use a two-way power splitter to split the RF output from USRP into two streams. Let the lengths of the wires through the first link be defined as l_1, and through the second link as l_2, respectively. An attenuator is connected at each of the links, correspondingly defined as α_1 and α_2, respectively. The received signals from the two links are then combined using a two-way power combiner.[7] The resultant signal is then fed to the EH module.

To proceed, we consider τ = 70%, α_2 = 0dB, and $l_1 - l_2$ = 15cm. A path difference of 15 cm at 915 MHz roughly translates to a phase difference of 160 degrees, since phase difference (in Radians) $\delta\phi = 2\pi/(\lambda\delta x)$ where δx is the path difference. Considering an OFDM transmission at the center frequency of f = 915 MHz, we show the effect of combining two approximately out-of-phase and differently attenuated OFDM signals in Fig. 15 while varying the values of path gains, i.e., α_1 (since α_2 is taken as 0). As anticipated, the WPT efficiency decreases with increasing values of α_1. Thus multipath effect caused by the phase difference between the two emulated paths can result in critical power losses in the case of OFDM, which eventually hampers both the information decoding and energy harvesting processes. Please note that OFDM is equipped with a cyclic prefix in order to counter such time spreads caused by multipaths, hence the severity of degradation in information decoding may not be as high as EH which gets affected due to the accumulation of signals with different phases.

VII. MAJOR OUTCOMES, APPLICATIONS AND INTERPRETIVE DISCUSSION - PART II

In this section, we present some of the practical application possibilities regarding the existing wireless communications systems. Ideally, the communications and WPT systems must coexist to provide the best gains in terms of their respective metrics. Correspondingly, we discuss herein three of the many distinct available possibilities where wireless communications and WPT systems can be harmonized. In this context, we consider an example of the proposed 5G NR non-standalone (NSA) setting to propose a feasible solution for the joint operation of the wireless communications and WPT systems. Next, we discuss another interesting aspect where the proposed methodology could be applicable in the IoT and non-terrestrial network (IoT-NTN) following the recent work in the 3GPP standardization process [25]. Finally, we illustrate another use case with a performance evaluation of the amplitude modulation (AM) scheme on the WPT process. The corresponding elaborative discussions follow.

1) *4G LTE-assisted 5G-NR in NSA consideration*: Following the recent trends about the 5G rollouts, it is important to note the wide deployment of NSA by the mobile operators [26]. This is primarily considered for faster roll-outs of the 5G network as full deployment of the StandAlone (SA) 5G network will take some time. From a mobile operator's perspective, the proposed

[6]Note that because of variable frequencies, the values of α will be different for both the cases.

[7]Note that herein, we have generated two paths only, more splitters and combiners with more number of outputs and inputs, respectively, may be considered for emulation of more than two paths. Optionally, a channel emulator can also be used.

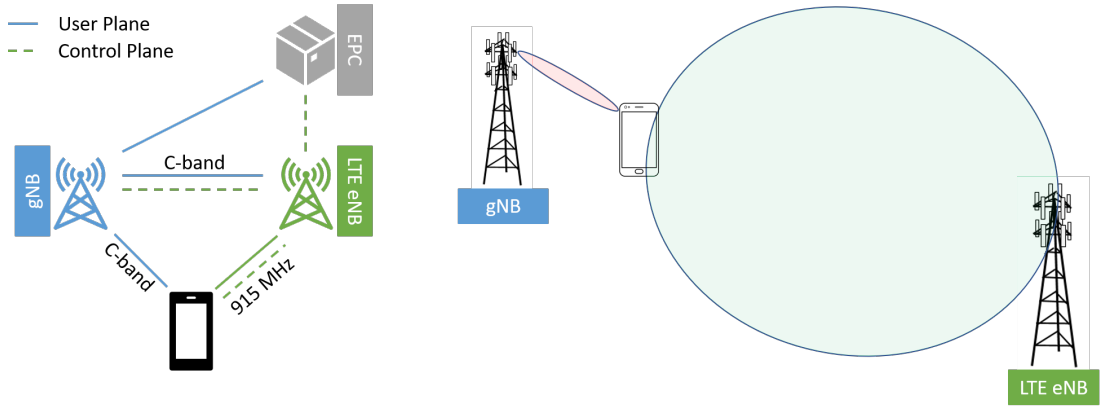

FIGURE 16. Depiction of traditional NSA system where 5G-NR is assisted by LTE to form the initial connection with the end-user. Lower frequency, which performs better for EH and has larger coverage, can be used for LTE anchor, while higher frequencies with lower coverage can be used for the 5G-NR connection.

NSA scheme enables them to leverage the already available network resources, e.g., 4G LTE, in contrast to the deployment of an overall new end-to-end SA 5G network. The main idea of NSA revolves around the aspect that the operators leverage their existing LTE/Voice over LTE (VoLTE) footprint to utilize their LTE installed base stations and increase capacity. A basic schematic of the NSA is depicted in Fig. 16.

To understand in simple terms, the deployment of 4G LTE is based on a large scale (also termed as “macrocells"), while the deployment of the proposed 5G-NR would be on a small scale (or “microcell"). Due to the wide availability of the 4G LTE base stations (BS), their consideration within the NSA scheme becomes crucial in practice. Under the NSA consideration, a 5G user can only create a communication link with the 5G-BS through a 4G LTE BS, even though the user is closer to its nearest 5G-BS. However, the adoption of different operational frequencies (about the 4G LTE and 5G-NR frameworks) opens up the space for the consideration of WPT, alongside the traditional information exchange in practical wireless systems. In this regard, the use of the C-band (3.4GHz and 4.2GHz) by the 5G-BS for the data channel and the 915 MHz band by 4G LTE-BS for the control channel could enable the exchange of information via 5G-BS and energy transmission via LTE-BS. This proposition follows from the results reported in Fig. 13. Following this prospect, the idea of SWIPT may be realized in practice accordingly.

2) *Incorporation of WPT in IoT-NTN systems*: Energy Harvesting assisted by the NSA mode of 5G-NR deployment can also be beneficial for the IoT devices which can harvest from the omnidirectional, and higher coverage transmission, of the 4G LTE anchor node. 3GPP RAN has started normative work on 5G-NR enhancements to support NTN, especially, the Transparent Mode of satellite operation is being considered where the gNB will be situated on the ground, and hence the radiated radio energy can be used for EH.
3) *Effect of AM signal on WPT Process*: The intuitive trend following the results of Fig. 13 suggest the use of low carriers for the WPT process, while the usage of high carrier frequencies for the information exchange process is well-established in wireless communications. This diverging tendency of carrier selection intrigues the authors to revisit some more basic modulation schemes, such as e.g., AM, for investigating the WPT process. In this regard, we performed additional experiments from the perspectives of varying the transmit power under variable attenuator conditions and varying the modulation index coefficient [27]. More details on this aspect are presented in Appendix B.

VIII. CONCLUSION

In this paper, we demonstrated the real-time analysis of WPT via various waveform designs viz., OFDM, square, triangular, sinusoidal, and sawtooth, transmitted over a wireless medium using an SDR. For the experimental tractability and for interpreting the V_{out} from the Powercast P21XXCSR-EVB EH module, we presented a mechanism to convert the received analog data to a digital interpretative format using MCP3008 ADC and RaspberryPi. The first phase of our results highlights that OFDM is the best suitable multi-carrier candidate among the considered set of waveform designs, while square waveform is found to be the ideal single carrier waveform for facilitating the EH process. In the second phase, we studied the effect on WPT with variable USRP transmit power, the separation distance between the USRP and EH antennas, the number of OFDM sub-carriers, and the multipath setting. As an application of OFDM, the effectiveness of fifth-generation-new radio (5G-NR) and fourth-generation long-term evolution (LTE) waveforms were also tested for the WPT mechanism. As interesting use cases, we provided discussions on the ap-

plications of this work in the LTE-assisted 5G-NR in NSA consideration, and incorporation of WPT in IoT-NTN systems. Additionally, the SWIPT/WPT suitability of other OFDM-based/alternative waveforms designed for 5G-and-beyond systems, such as filtered-OFDM, weighted overlap and add based OFDM (WOLA-OFDM), circularly pulse-shaped precoding for OFDM, and Generalized frequency division multiplexing (GFDM), will be investigated in future. It is also well-known that OFDM possesses both severe out-of-band emission and high peak-to-average-power ratio (PAPR) causing a nonlinear distortion via a power amplifier (PA). In this regard, addressing the two above-mentioned factors that affect the WPT and EH performances would be another interesting prospect to study in the future.

.

REFERENCES

[1] R. Varshney, "Transporting information and energy simultaneously," in *2008 IEEE Int. Symp. on Information Theory*, 2008, pp. 1612–1616.
[2] B. Clerckx *et al.*, "Fundamentals of Wireless Information and Power Transfer: From RF Energy Harvester Models to Signal and SystemDesigns," *IEEE J. Sel. Areas Commun.*, vol. 37, no. 1, pp. 4–33, 2019.
[3] N. Ayir, M. F. Trujillo Fierro, T. Riihonen, and M. Allén, "Experimenting Waveforms and Efficiency in RF Power Transfer," in *2019 IEEE MTT-S International Microwave Symposium (IMS)*, 2019, pp. 1140–1143.
[4] K. Yamaguchi, T. Hirata, and I. Hodaka, "Using Square Wave Input for Wireless Power Transfer," *International Journal of Electrical & Computer Engineering (2088-8708)*, vol. 6, no. 1, 2016.
[5] N. Shanin, L. Cottatellucci, and R. Schober, "Markov Decision Process Based Design of SWIPT Systems: Non-Linear EH Circuits, Memory,and Impedance Mismatch," *IEEE Trans. Commun.*, vol. 69, no. 2, pp. 1259–1274, 2021.
[6] N. Ayir and T. Riihonen, "Impact of Software-Defined Radio Transmitter on the Efficiency of RF Wireless Power Transfer," in 2020 IEEE Wireless Power Transfer Conference (WPTC), 2020, pp. 83–86.
[7] A. Boaventura *et al.*, "Boosting the Efficiency: Unconventional Waveform Design for Efficient Wireless Power Transfer," in IEEE Microw. Mag., vol. 16, no. 3, pp. 87–96, 2015.
[8] B. Clerckx and E. Bayguzina, "Waveform design for wireless power transfer," IEEE Trans. Signal Proc., vol. 64, no. 23, pp. 6313–6328, Dec. 2016.
[9] J. Kim, B. Clerckx, and P. D. Mitcheson, "Signal and system design for wireless power transfer : Prototype, experiment and validation," IEEE Trans. Wireless Commun., pp. 1–1, 2020.
[10] Y. Zeng, B. Clerckx, and R. Zhang, "Communications and signals design for wireless power transmission," IEEE Trans. Commun., vol. 65, no. 5, pp. 2264–2290, May 2017.
[11] Y. Ma, Z. Luo, C. Steiger, G. Traverso, and F. Adib, "Enabling deep-tissue networking for miniature medical devices," in Proc. Conference of the ACM Special Interest Group on Data Communication (SIGCOMM), Aug. 2018.
[12] A. J. S. Boaventura, A. Collado, A. Georgiadis, and N. B. Carvalho, "Spatial power combining of multi-sine signals for wireless power transmission applications," IEEE Trans. Microw. Theory Techn., vol. 62, no. 4, pp. 1022–1030, Apr. 2014.
[13] "Ettus Research," https://www.ettus.com/all-products/ub210-kit/, Accessed: 2021-07-29.
[14] "Vert-2450," https://www.ettus.com/all-products/vert2450/, Accessed:2021-07-29.
[15] "GNU Radio," https://www.gnuradio.org/, Accessed: 2021-07-29.
[16] B. Bloessl, M. Segata, C. Sommer, and F. Dressler, "An IEEE 802.11a/g/p OFDM Receiver for GNU Radio," in *Proceedings of the second workshop on Software radio implementation forum*, 2013, pp. 9–16.
[17] Powercast Corporation, P21XXCSR-EVB, https://www.powercastco.com/documentation/p21xxcsr-evb-datasheet/, Accessed: 2021-07-29.
[18] H. Aboueidah *et al.*, "Characterization of RF energy harvesting at 2.4 GHz," in *2017 24th IEEE International Conference on Electronics, Circuits and Systems (ICECS)*, 2017, pp. 446–449.
[19] "MCP3008 ADC," https://cdn-shop.adafruit.com/datasheets/MCP3008.pdf, Accessed: 2021-07-29.
[20] "RaspberryPi-v4," https://www.raspberrypi.org/products/raspberry-pi-4-model-b/, Accessed: 2021-02-28.
[21] H. T. Friis, "A note on a simple transmission formula," *Proceedings of the IRE*, vol. 34, no. 5, pp. 254–256, 1946.
[22] W. Yu and R. Lui, "Dual Methods for Nonconvex Spectrum Optimizationof Multicarrier Systems,"IEEE Trans. Commun., vol. 54, no. 7, pp.1310–1322, 2006.
[23] A. Yazar and H. Arslan, "A Flexibility Metric and Optimization Methods for Mixed Numerologies in 5G and Beyond," IEEE Access, vol. 6, pp.3755–3764, 2018.
[24] L. Marijanović, S. Schwarz, and M. Rupp, "Multiplexing Services in 5G and Beyond: Optimal Resource Allocation Based on Mixed Numerology and Mini-Slots," IEEE Access, vol. 8, pp. 209537–209555, 2020.
[25] 3GPP TR 38.821, "Solutions for NR to support Non-Terrestrial Networks (NTN)" https://portal.3gpp.org/desktopmodules/Specifications/SpecificationDetails.aspx?specificationId=3525, Accessed: 2021-08-09.
[26] J. Lowe, "5G NR Non-standalone vs. 5G Standalone: What you need to know," Infovista Blog, Aug. 6, 2020. https://www.infovista.com/5g-nr-non-standalone, Accessed: 2021-07-29.
[27] TutorialsPoint, "Amplitude Modulation," https://www.tutorialspoint.com/analog_communication/analog_communication_amplitude_modulation.htm, Accessed: 2021-07-29.
[28] Wikipedia, "Sine wave," https://en.wikipedia.org/wiki/Sine_wave, Accessed: 2021-07-30.
[29] Wikipedia, "Square wave," https://en.wikipedia.org/wiki/Square_wave, Accessed: 2021-07-30.
[30] Wikipedia, "Triangle wave," https://en.wikipedia.org/wiki/Triangle_wave, Accessed: 2021-07-30.
[31] Wikipedia, "Sawtooth wave," https://en.wikipedia.org/wiki/Sawtooth_wave, Accessed: 2021-07-30.
[32] Wikipedia, "Orthogonal frequency-division multiplexing," https://en.wikipedia.org/wiki/Orthogonal_frequency-division_multiplexing, Accessed: 2021-07-30.

APPENDIX A INTUITIVE DISCUSSION ON EFFECT OF VARIOUS WAVEFORMS ON WPT PROCESS

In this section, we discuss the intuitive reasoning behind the consideration of various waveforms and their effects on the WPT operation. To proceed, let us put forth relevant mathematical equations to represent a different types of considered waveforms, as follows

1) *Sinusoidal Waveform*: A smooth periodic oscillation mostly characterizes a continuous sine-wave, whose most basic form is defined as a function of time (t) as follows

$$x(t) = A\sin(2\pi ft + \phi) = A\sin(\omega t + \phi), \quad (2)$$

where A is defined as the amplitude, f as the frequency, $\omega = 2\pi f$ is the angular frequency, and ϕ is defined as the phase. [28]

2) *Square Waveform*: In general, a square wave is defined as simply the sign function i.e., $sgn(\cdot)$, of a sinusoid, written as follows [29]

$$x(t) = sgn(\sin(2\pi ft)), \quad (3)$$

$$v(t) = sgn(\cos(2\pi ft)), \quad (4)$$

where the output is 1 in case sinusoid is positive, while the output is -1 in case sinusoid is negative. The output is 0 at the discontinuities. A square wave can also be defined with respect to the Heaviside step function $u(t)$

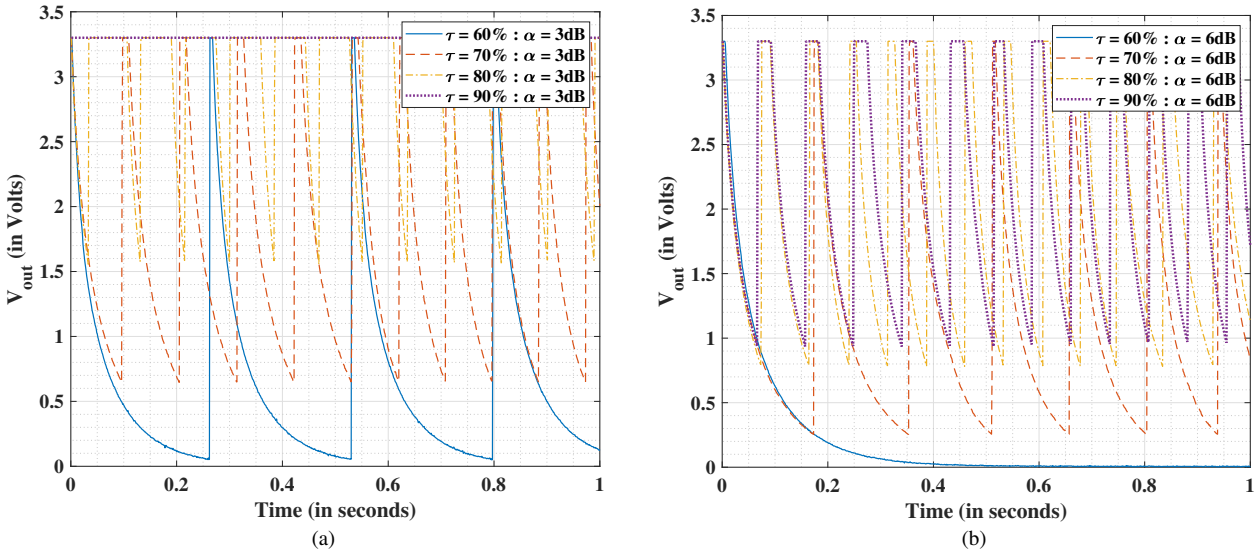

FIGURE 17. The effectiveness of AM signal in terms of WPT is depicted herein for various values of USRP transmit power (τ) values, for (a) α = 3dB and (b) α = 6dB, with f = 915 MHz and μ = 1.

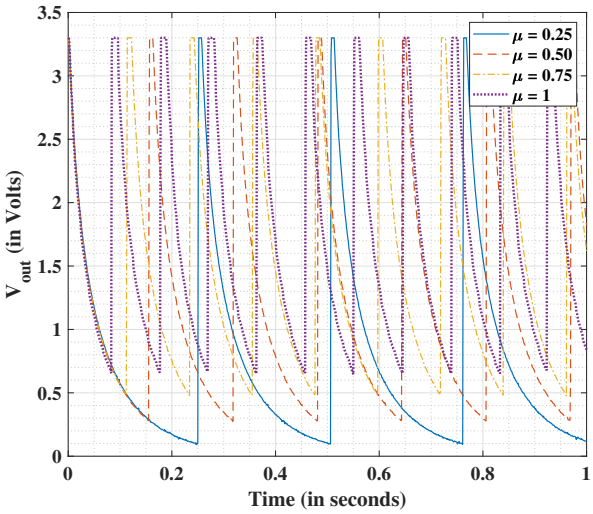

FIGURE 18. Comparison of various values of modulation index (μ) facilitating WPT, with τ = 70% and α = 3dB.

or the rectangular function $\Pi(t)$, represented as

$$x(t) = 2\left[\sum_{n=-\infty}^{\infty} \Pi\left(\frac{2(t-nT)}{T} - \frac{1}{2}\right)\right] - 1,$$

$$= 2\sum_{n=-\infty}^{\infty}\left[u\left(\frac{t}{T} - n\right) - u\left(\frac{t}{T} - n - \frac{1}{2}\right)\right] - 1. \quad (5)$$

3) *Triangular Waveform*: A triangular wave of period p that spans the range $[-1, 1]$ is defined as [30]

$$x(t) = 2\left|2\left(\frac{t}{p} - \left\lfloor\frac{t}{p} + \frac{1}{2}\right\rfloor\right)\right|, \quad (6)$$

where $\lfloor\cdot\rfloor$ is the floor function.

4) *Sawtooth Waveform*: The general form of sawtooth wave function ranging between -1 to 1 and with a period p is given by [31]

$$x(t) = 2\left(\frac{t}{p} - \left\lfloor\frac{t}{p} + \frac{1}{2}\right\rfloor\right). \quad (7)$$

Note that the previously defined triangular wave function is an absolute value of the sawtooth wave function. It is noteworthy that the sawtooth function has the same phase as the sinusoid function.

5) *OFDM Waveform*: OFDM is a well-known multi-carrier setting. Assuming that if N sub-carriers are in-use and each sub-carrier is modulated using M alternative symbols, the OFDM symbol alphabet consists of M^N combined symbols. In order to avoid intersymbol interference in multipath fading channels, the OFDM block is prefixed with a guard interval of length T_g, wherein a cyclic-prefix is added to the transmit signal in the interval $(T - T_g \leq t < T)$. Therefore, the (low-pass equivalent) OFDM signal with cyclic prefix is expressed as

$$x(t) = \sum_{n=0}^{N-1} S_n \exp\left(j2\pi nt/T\right), -T_g \leq t < T. \quad (8)$$

where S_n are the data symbols, N is the number of subcarriers, and T is the OFDM symbol time.

The nature and behavior of the wave functions mentioned above are well-known with respect to time. Considering the WPT process, a waveform with a more frequently occurring crest/trough would be better suited from a general intuition. Ideally, the direct current (DC) component required to charge a battery should be nearly a constant value. This could be ensured by using such type of waveform which can provide a DC-type of output. To understand better, consider the discrete

samples of all the waveforms within a time-period. We note that in a square wave, a large part of the signal is at a high state within the said time-period. Similarly, in the case of OFDM (probably with a large number of sub-carriers), the outcome with discrete samples would yield a rectangular type of output which is best suited for the WPT process. In the case of the sinusoid, triangular and sawtooth, the discrete samples are unable to provide a consistent output and hence the EH module should require a larger time duration to extract energy from these signals in comparison to OFDM and square waveforms.

APPENDIX B INVESTIGATION OF AM BASED WPT

In this section, we discuss the effect of AM signal on the WPT process. We first recollect the mathematical framework for generating an AM signal. Following the time-domain representation of the waves, let the modulating signal be mathematically defined as,

$$m(t) = A_m \cos(2\pi f_m t), \tag{9}$$

and the carrier signal be represented as,

$$c(t) = A_c \cos(2\pi f_c t), \tag{10}$$

where, A_m and A_c are the amplitude of the modulating signal and the carrier signal respectively; and f_m and f_c are the frequency of the modulating signal and the carrier signal respectively.

Then, the equation of AM wave will be given by

$$s(t) = [A_c + A_m \cos(2\pi f_m t)] \cos(2\pi f_c t). \tag{11}$$

After some further simplifications, (11) can be rewritten as

$$s(t) = A_c[1 + \mu \cos(2\pi f_m t)] \cos(2\pi f_c t), \tag{12}$$

where $\mu = \frac{A_m}{A_c}$ is defined as the modulation index. The selection of μ determines the characteristic of AM wave. For instance, if this value is less than 1, i.e., the modulation index is 0.5, then AM signal experiences under-modulation, whereas in case the value of the modulation index is greater than 1, i.e., 1.5 or so, then the wave will be an over-modulated wave. For a perfect modulation, the value of modulation index should be 1, which implies the percentage of modulation should be 100%. We consider these cases in further analysis.

Regarding the experimental deployment, an AM wave is generated according to (12) with f_m = 100 kHz and f_c = 2 MHz. Then, another carrier centered at 915 MHz is superimposed to the AM waveform obtained above to respect the band limitations of the EH module. We follow a similar process as depicted in Fig. 7. In this vein, we first experiment with the variation of the USRP transmit power (τ) and the attenuator (α), with corresponding results depicted in Fig. 17. We observe that the signal with higher transmit power outperforms the others in both Fig. 17 (a) and Fig. 17 (b). However, the charging of the capacitor is less frequent when the distance between the USRP and EH module is increased virtually with the help of α, as inferred from both the figures. The performance of AM can also be considered reasonable for WPT at high values of τ. Next, we perform an investigation with variable μ while considering τ = 70% and α = 3dB. The corresponding results are reported in Fig. 18. We observe that a fully modulated signal, i.e., AM with μ = 1, would be the best-suited waveform for WPT in this case.

SUMIT GAUTAM (S'14-M'20) received the B.Tech. degree (Hons.) in electronics and communication engineering from the LNM Institute of Information Technology (Deemed University), Jaipur, India, in 2013, and the M.S. degree in electronics and communication engineering by research from the International Institute of Information Technology Hyderabad (Deemed University), Hyderabad, India, in 2017, and the Ph.D. degree in computer science from the Interdisciplinary Centre for Security, Reliability, and Trust (SnT), University of Luxembourg, Luxembourg, in 2020. He is currently working as a Research Associate/Postdoctoral Researcher with the Interdisciplinary Centre for Security, Reliability, and Trust (SnT), University of Luxembourg. His research interests include simultaneous wireless information and power transfer, caching, optimization methods, hybrid active-and-passive cooperative communications, and precoding for multi-group multicast systems.

SUMIT KUMAR (S'14-M'19) received the B.Tech and M.S. in Electronics & Communication Engineering from Gurukula Kangri University, Haridwar, India (2008) and the International Institute of Information Technology, Hyderabad, India (2014), respectively, and the Ph.D. from Eurecom (France) in 2019. Currently, he is working as a Research Associate at the Interdisciplinary Centre for Security, Reliability, and Trust (SnT), University of Luxembourg. His research interests are in wireless communication, interference management, Integration of 5G with Non-Terrestrial-Networks and Software Defined Radio prototyping.

SYMEON CHATZINOTAS (S'06-M'09-SM'13) is currently the Deputy Head of the SIGCOM Research Group, Interdisciplinary Centre for Security, Reliability, and Trust, University of Luxembourg, Luxembourg, and Visiting Professor at the University of Parma, Italy. He received the M.Eng. degree in telecommunications from the Aristotle University of Thessaloniki, Thessaloniki, Greece, in 2003, and the M.Sc. and Ph.D. degrees in electronic engineering from the University of Surrey, Surrey, U.K., in 2006 and 2009, respectively. He was involved in numerous Research and Development projects for the Institute of Informatics Telecommunications, National Center for Scientific Research Demokritos, the Institute of Telematics and Informatics, Center of Research and Technology Hellas, and the Mobile Communications Research Group, Center of Communication Systems Research, University of Surrey. He has over 300 publications, 3000 citations, and an H-Index of 28 according to Google Scholar. His research interests include multiuser information theory, co-operative/cognitive communications, and wireless networks optimization. He was a co-recipient of the 2014 IEEE Distinguished Contributions to Satellite Communications Award, the CROWNCOM 2015 Best Paper Award, and the 2018 EURASIC JWCN Best Paper Award.

BJÖRN OTTERSTEN (S'87-M'89-SM'99-F'04) was born in Stockholm, Sweden, in 1961. He received the M.S. degree in electrical engineering and applied physics from Linköping University, Linköping, Sweden, in 1986, and the Ph.D. degree in electrical engineering from Stanford University, Stanford, CA, USA, in 1990. He has held research positions with the Department of Electrical Engineering, Linköping University, the Information Systems Laboratory, Stanford University, the Katholieke Universiteit Leuven, Leuven, Belgium, and the University of Luxembourg, Luxembourg. From 1996 to 1997, he was the Director of Research with ArrayComm, Inc., a start-up in San Jose, CA, USA, based on his patented technology. In 1991, he was appointed a Professor of signal processing with the Royal Institute of Technology (KTH), Stockholm, Sweden. From 1992 to 2004, he was the Head of the Department for Signals, Sensors, and Systems, KTH, and from 2004 to 2008, he was the Dean of the School of Electrical Engineering, KTH. He is currently the Director for the Interdisciplinary Centre for Security, Reliability and Trust, University of Luxembourg.

He was a recipient of the IEEE Signal Processing Society Technical Achievement Award in 2011 and the European Research Council advanced research grant twice, in 2009-2013 and in 2017-2022. He has co-authored journal papers that received the IEEE Signal Processing Society Best Paper Award in 1993, 2001, 2006, and 2013, and seven IEEE conference papers best paper awards. He has served as an Associate Editor for the IEEE TRANSACTIONS ON SIGNAL PROCESSING and the Editorial Board of the IEEE Signal Processing Magazine. He is currently a member of the editorial boards of EURASIP Signal Processing Journal, EURASIP Journal of Advances Signal Processing and Foundations and Trends of Signal Processing. He is a fellow of EURASIP.